Indian Journal of Science and Technology, *Vol 11(19), DOI: 10.17485/ijst/2018/v11i19/122884, May 2018*
ISSN (Print) : 0974-6846
ISSN (Online) : 0974-5645

Superparamagnetic $MnFe_2O_4$ and $MnFe_2O_4$ NPs/ABS Nanocomposite: Preparation, Thermal Stability and Exchange Bias Effect

Asma-M AlTurki*

Department of Chemistry, Facility of Science, University of Tabuk, Tabuk, P.B. 1247 Zip code 71431, Saudi Arabia; aalturky@ut.edu.sa

Abstract

Objectives: Manganese Ferrite nanoparticles are a current hot topic in medicine and pharmaceutics. In the current investigation, $MnFe_2O_4$ NPs/ABS Nanocomposite have been successfully synthesized via Co-precipitation method process. **Methods/Statistical Analysis:** Manganese Ferrite nanoparticles ($MnFe_2O_4$ (MF) NPs) were synthesized by the Co-precipitation method then annealing at 400°C. A nanocomposite of $MnFe_2O_4$ with acrylonitrile (A) butadiene (B) styrene (S) (MF/ABS) was prepared. Scanning electron microscopy (SEM), energy dispersive analysis X-ray (EDAX) and transition electron microscopy (TEM) were used to characterize the morphology and particle size of the MF NPs and MF/ABS nanocomposite. **Findings:** The nano-powders obtained have a spherical structure and particle size of approximately 8 nm. The optical properties were studied by UV-Vis spectroscopy to estimate the band gap of the MF NPs and MF/ABS nanocomposite. The magnetic properties of the MF NPs and MF/ABS nanocomposite were investigated using a vibrating sample magnetometer (VSM). We found that the MF NPs exhibit a superparamagnetic behaviour. The saturation magnetization Ms (8.4277E-3 emu/g) and coercivity Hci (91.208 G) at room temperature for the MF/ABS nanocomposites were higher than Ms and Hci for the MF NPs. The exchange bias effect appears in the MF/ABS nanocomposite. The thermal results show that the glass transition temperature (Tg) of the MF/ABS nanocomposites is 108.54 ºC. **Application/Improvements:** Adding 10% of MF NPs to ABS polymer enhance ABS thermal properties and change ABS magnetic properties.

Keywords: Exchange Bias Effect, Nanocomposite, Superparamagnetic, Thermal Stability, ABS

1. Introduction

Magnetic nanoparticles are a current hot topic in medicine and pharmaceutics[1]. Nanoparticles promise matchless improvements for numerous sectors, such as medicine, energy, biosensors, and materials[2-5]. These materials have a very wide range of applications due to their unique combination of high magnetization and paramagnetic behaviour. Magnetic nanoparticles can be used as drug delivery systems for magnetic-induced tumour treatment[6]. Nanoparticle properties are incredibly consistent in composition, morphology, and size depending on the preparation method[7].

Manganese ferrite ($MnFe_2O_4$) nanoparticles show excellent magnetic, mechanical, and luminescent properties in contrast with other magnetic ferrite nanoparticles[8-10]. Manganese ferrite $MnFe_2O_4$ has exceptional magnetic properties, such as moderate saturation magnetization, low coercivity, moderate saturation magnetization, and chemical stability[11]. When multiple layers of a ferromagnet connect with an antiferromagnet, a shift of the hysteresis loop over the magnetic field axis called exchange bias can happen. This phenomenon is observed to enhance the coercivity (Hci)[12].

There are many methods for synthesizing nanoparticles such as hydrothermal, sol-gel, solvothermal, hydrothermal and co-precipitation methods. Co-precipitation is

*Author for correspondence

a promising method for preparing nano ferrites due to increased purity, reactivity, and homogeneity. The co-precipitation method is simple and low cost, and it also helps control the particle size[13]. Magnetic nano-sized particles have a unique collection of high magnetization and a paramagnetic property[14].

Acrylonitrile butadiene styrene (ABS) is a two-phase polymer comprising polybutadiene and styrene-acrylonitrile as a copolymer. ABS has important mechanical properties such as impact resistance and toughness. Adding filler to ABS can provide a chance to compete with other polymers to finds applications in different fields such as appliances, automotive applications, packaging, pipes and so on[15].

In the present work, $MnFe_2O_4$ NPs were synthesized by the co-precipitation method, and then ABS was mixed with 10% $MnFe_2O_4$ NPs. The study of the thermal properties employed Differential Scanning Calorimetry (DSC) and Thermo Gravimetric Analysis (TGA), and the morphology study was performed using Scanning Electron Microscopy (SEM), Energy Dispersive Analysis X-ray (EDAX) and Transition Electron Microscope (TEM). The optical properties were studied by UV-Vis spectroscopy to estimate the band gap of the MF NPs and MF/ABS nanocomposite. Vibrating Sample Magnetometer (VSM) techniques were used to characterize and detect the relationship of the structural properties of ABS and the magnetic properties to be used in different technological applications.

2. Experimental

2.1 Material and Methods

Manganese chloride tetrahydrate ($MnCl_2.4H_2O$), ferric chloride ($FeCl_3$), sodium hydroxide (NaOH) were purchased from Sigma Aldrich Co. Ltd. (USA); Acrylonitrile butadiene styrene (ABS) from SABIC, Saudi Arabia; HPLC-grade Dichloromethane was purchased from Fisher Chemical; and distilled water was used.

2.2 Synthesis of MF NPs Powder

MF NPs powder was prepared by a Co-precipitation method using a 50 ml solution with 1.48 g of $MnCl_2.4H_2O$ and a 50 ml solution is containing 0.60 gm of $FeCl_3$. These solutions were mixed, and then a 6 molar NaOH solution was added drop by drop (the pH of the medium was approximately 11) at room temperature. After stirring at the same temperature for 10 min and then heating it to 90˚C for 30 minutes, the obtained precipitate was washed several times with distilled water; at this time a dry, black powder was obtained. Finally, the dry, black powder was heated at 400°C˚ for 4 hours.

2.3 Preparation of MF/ABS Nanocomposite Films

One gram of ABS was dissolved in 10 ml dichloromethane and stirred for 30 min; after that we prepared a 10% MF/ABS nanocomposite by mixing calcined MF NPs with the above solution. Then, the mixture was cast at room temperature in a petri dish until it dried and formed the MF/ABS nanocomposite.

2.4 Characterization and Measurements

The morphology and elemental contents were determined by Scanning Electron Microscopy (SEM) and Energy Dispersive X-ray Analysis (EDAX), with accelerating voltage=20.0 kV, working distance=10 mm, spot size=4.5 (EDX), and 2.0-3.0 (SEM). Transmission Electron Microscopy (TEM) studies were performed (TEM, JEOL JEM-3010, 3 kv). The samples for TEM were prepared by making a suspension from the powder in deionized water. A drop of the suspension was placed into the carbon grid and left to dry. The optical properties of the MF NPs and MF/ABS nanocomposite structures were characterized by UV-vis absorption from 200-800 nm (UV–Vis spectrophotometer Model JASCO V-670, Japan instrument). DSC curves were obtained using a TA Instrument DSC Q1000 (V9.9 Build 303), and the thermal behaviour of the prepared samples was examined by TGA Q500 V20.13 Build 39 to assess the stability of the MF/ABS nanocomposite. Vibrating Sample Magnetometer (VSM) techniques were used to study the magnetic properties of the prepared samples by applying a field up to 20 KG at room temperature.

3. Results and Discussion

3.1 Characterization MF NPs Powder

- **EDAX**

  An EDAX analysis was performed on multiple particles in area mode (~25-50 m2) using an EDAX

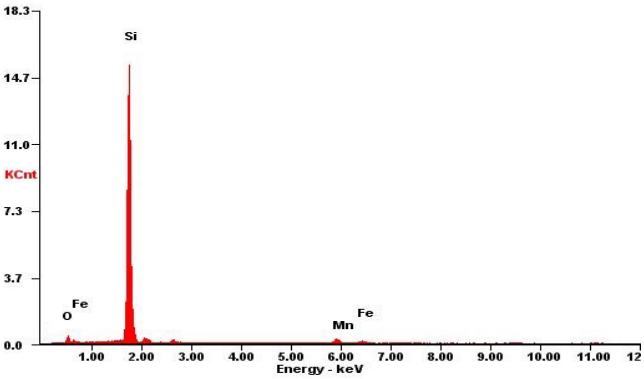

Figure 1. EDAX result of the MF NPs.

Genesis XM4 system attached to SEM. The elemental contents for the MF NPs determined are shown in Figure 1. The results of EDAX revealed high oxygen content 46.40% in the samples examined. We also demonstrate the presence of Mn and Fe, the contents of which amounted to 34.87% and 18.73%, respectively. In the EDAX spectrum, a silicon peak appeared, generated when all of the energy of an incoming X-ray was transformed into electron-hole pairs. A Si Kα X-ray was produced from the silicon detector crystal; the energy measured for the incoming X-ray was reduced by the magnitude of the Si Kα X-ray, i.e., 1.74 keV, and a Si escape peak was detected in the EDAX spectrum.

- **SEM**

  The SEM micrographs of the MF NPs are shown in Figure 2. SEM images of the MF NPs, which were found, have a spherical shape.

- **TEM**

  TEM images were used to study the microstructures of the MF NPs. The SEM results were well supported

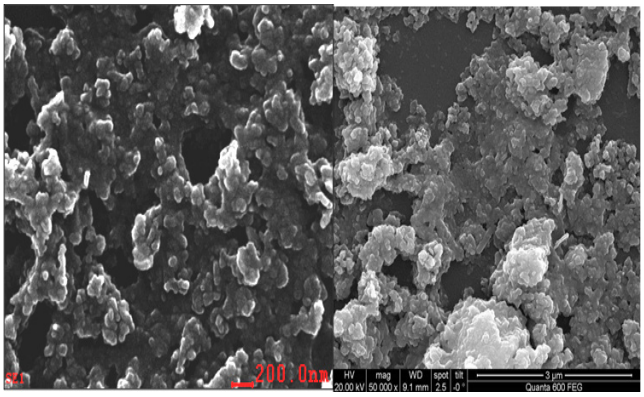

Figure 2. SEM images of the MF NPs.

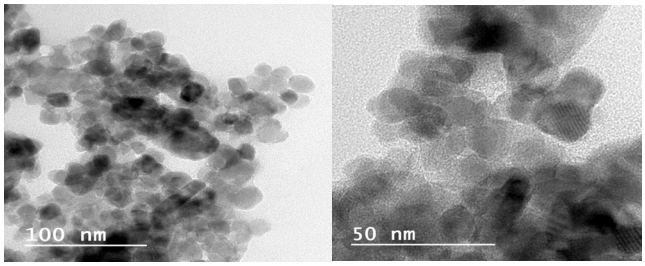

Figure 3. The TEM images for MF NPs.

by the TEM measurements of the MF NPs. Figure 3 shows the representative TEM images of the MF NPs. The morphology of the MF NPs was found to be nearly spherical, and the TEM analysis shows the particles size of the MF NPs to be 8 nm. The TEM results indicated by the dark sites may be due to the accumulation of nanoparticles with a particle size smaller than 8 nm[15].

3.2 Optical Properties

The optical absorption spectrum the MF NPs and MF/ABS nanocomposite was examined using a UV-Vis

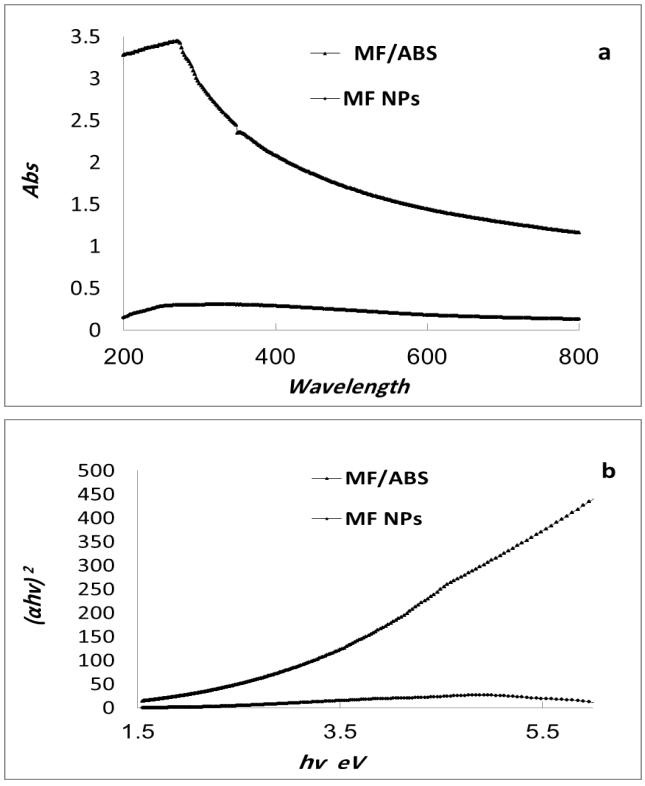

Figure 4. The optical absorption spectra for the MF NPs and MF/ABS nanocomposite(a) and the plot of (αhν)2 versus hν for the MF NPs and MF/ABS nanocomposite(b).

spectrophotometer in the wavelength range from 200 to 800 nm using UV-Vis spectrophotometer Model JASCO V-670, Japan. Figure 4a shows the absorption peaks for the MF NPs and MF/ABS nanocomposite. To determine the optical band gap of the MF NPs and MF/ABS nanocomposite, we plotted $(\alpha hv)^2$ versus hv, where hv is the photon energy and α is the absorption coefficient[16]. A plot is shown in Figure 4b. The band gap of the MF NPs was evaluated from the plot to be approximately 1.6 eV, but for the MF/ABS nanocomposite shown in blue it was 2.7 eV. The blueshift is due to adding the nanoparticle filler to the polymer matrix[17].

3.3 Thermal Analysis

The thermal properties of the MF/ABS nanocomposite were studied by thermogravimetric analysis (TGA) and a differential scanning calorimeter (DSC). As shown in Figure 5, DSC was scanned for 2.62 mg of MF/ABS nanocomposite from 40°C to 200°C under an inert atmosphere at a rate of 10°C min^{-1} with two heating stages. The first heating stage was followed by a cooling process and a second heating stage. The glass transition temperature (Tg) value was studied from the second heating stage for the MF/ABS nanocomposite. The Tg value showed little change in the Tg value for the MF/ABS nanocomposite (108.54°C) compared with the Tg values of pure ABS (102°C)[14].

A TGA analysis used to determine the thermal stability. It was performed by heating the MF/ABS nanocomposite from room temperature to 800°C under air and an inert atmosphere (N_2) with a heating rate of 10°C min^{-1} and flow rate of 50 ml/min. The degradation of pure ABS began at 340°C with the production of butadiene; then, aromatics were absorbed as a second product of degradation at 350°C. At the final stage of 400°C the evolution of acrylonitrile is absorbed[18]. For our sample MF/ABS nanocomposite, the TGA result in Figure 6 shows that the thermal properties of ABS were enhanced by adding

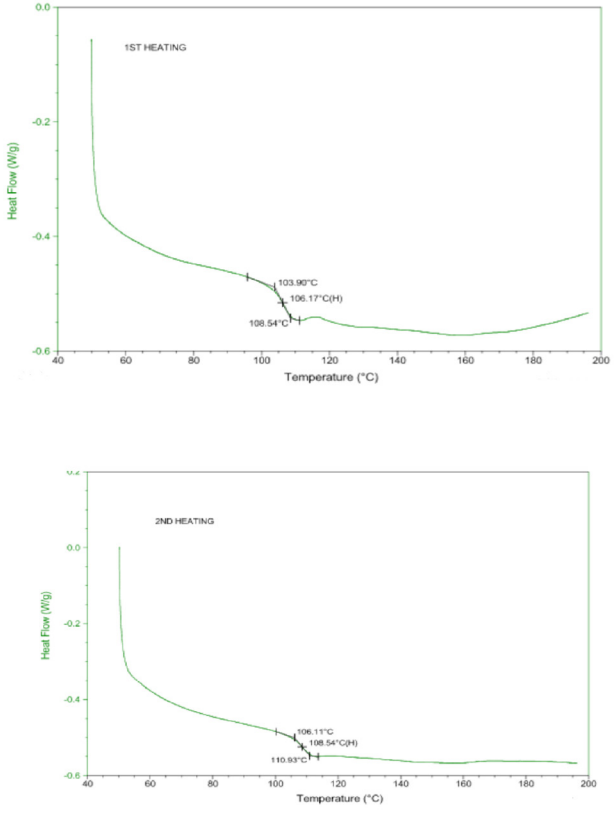

Figure 5. DSC analysis for the MF/ABS nanocomposite during the first and second heating.

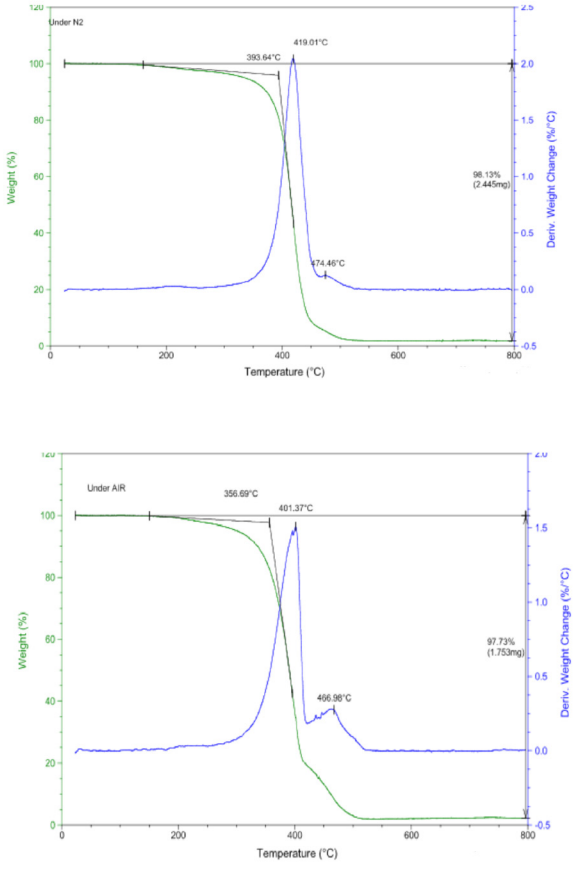

Figure 6. TGA analysis for the MF/ABS nanocomposite under an inert atmosphere (N2) and AIR

10% nanofillers (MF NPs)[14]; the first degradation stage of the MF/ABS nanocomposite started at 393.64°C, and the last stage of degradation started at 474.46°C under N_2, ranging between 356.69°C and 466.98°C under air. The degradation operations conducted in a two stage suggest a good interaction between the MF NPs and ABS[19]. Furthermore, the thermal decomposition under N_2 and air showed only one stage of weight loss; the weight loss and residual weight of the MF/ABS nanocomposite for the TGA analysis under N_2 were found to be 98.13% and 1.87%, respectively, and it was found to be 97.73% and 2.63%, respectively, under air.

3.4 VSM

When the particle size of magnetite particles decreases below 30 nm, the magnetic properties change[20]. Figure 7 presents the hysteresis loop of the MF NPs and MF/ABS nanocomposite measured at room temperature with 20 KG as the maximum magnetic field applied by a vibrating sample magnetometer (VSM). For the MF NPs the saturation magnetization (Ms) was 4.1869 emu/g, the coercivity (Hci) was 34G and the squareness was 1.44 E-2; for the MF/ABS nanocomposites the saturation magnetization (Ms) was 8.42E-3 emu/g, and the coercivity (Hci) was 91.208 G at room temperature. The absence of a hysteresis loop and the low value of coercivity and remanent magnetization at room temperature show that the nanoparticles exhibit a superparamagnetic behaviour[21]. The superparamagnetic phenomena are size-dependent and demonstrated by the small surface effect[22,23]. In general, magnetic properties change with variations in the shape, particle size, crystallinity and so on. The Ms Value decreased with the reduction of particle size. The Ms Value of bulk $MnFe_2O_4$ was 80 emu/g, and it was higher than the Ms Value of the MF NPs prepared in this work[24]. The saturation magnetization of the MF NPs was higher than those obtained for the MF/ABS nanocomposite (10%). The results also indicate that the distribution of the magnetic nanoparticles into the polymer matrix caused the coercivity to increase due to the interactions between the ABS chains and MF NPs. In our results, the coercivity (Hci) and remanent magnetization (Mr) were very small; we can explain this by the squareness ratio, which is defined as the ratio between remanence and saturation (Mr/Ms). Superparamagnetic materials have a Mr/Ms value << 0.01. The squareness of the MF NPs and MF/ABS nanocomposite was 1.44 E-2 and 38.27 E-3, respectively, indicating no squareness. Moreover, it exhibits an S-shape, confirming that our samples are superparamagnetic[25]. The VSM result for the MF/ABS exhibited negative remanent magnetization (NRM) as shown in Figure 7. NRM, also known as an inverted hysteresis loop, has been observed due to the different connectivity of magnetic nanometre-scale particles (superparamagnetic $MnFe_2O_4$ NPs) and ferromagnetic thin film (ABS)[26,27]. These effects are called exchange bias[28].

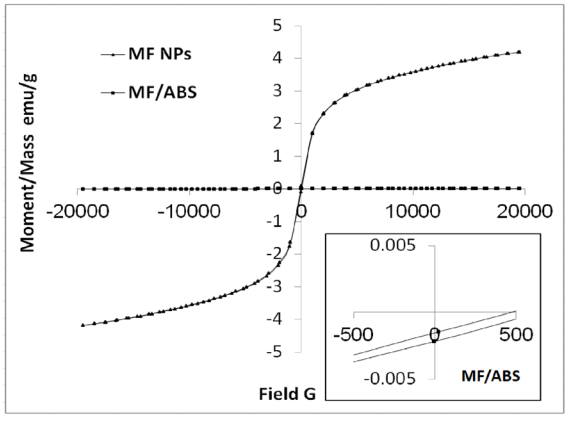

Figure 7. VSM analysis for the MF/ABS nanocomposite.

4. Conclusions

$MnFe_2O_4$ (MF) NPs were synthesized by the co-precipitation method with nearly spherical nanoparticles. The average partial size of the $MnFe_2O_4$ (MF) NPs was approximately 8 nm. The band gap value of the MF/ABS nanocomposite was higher than that of the MF NPs. The thermal properties of the pure ABS polymer were enhanced by adding MF NPs as nanofillers. Degradation started at 474°C under N_2 and ranged between 356.69°C and 466.98°C under air. The hysteresis loop of the MF NPs exhibited a superparamagnetic behaviour, and the MF/ABS nanocomposite exhibited the exchange bias effect due to the different connectivity of superparamagnetic of the NPs and ferromagnetic thin film.

5. Acknowledgments

The author would like to show her gratitude to Mr. Abdullah Almayouf from Analytical Lab at SABIC

Technology & Innovation Center for his inspiring help in thermal Analysis for the samples.

6. Reference

1. Lu AH, Salabas EL, Schuth F. Magnetic nanoparticles: Synthesis, protection, functionalization, and application. Angewandte Chemie International Edition. 2007; 46(8):1222-44. Crossref. PMid:17278160.
2. Mahmoudi M, Simchi A, Imani M, Stroeve P, Sohrabi A. Templated growth of superparamagnetic iron oxide nanoparticles by temperature programming in the presence of poly(vinyl alcohol. Thin Solid Films. 2010; 518(15): 4281-9. Crossref.
3. Challa SSR, Kumar. Biofunctionalization of Nanomaterials. Wiley-VCH: Weinheim. 2005; p. 72-98.
4. Isa K, Mustafa A, Taher D, Mohammad RG, Peir HK. Superparamagnetic Iron Oxide Nanoparticles Coated with PEG/PEI for Biomedical Applications: A Facile and Scalable Preparation Route Based on the Cathodic Electrochemical Deposition Method. Advances in Physical Chemistry. 2017; 2017:1-7.
5. Binh TTP, Emily KC, Nguyen THP, Byung JK, Emily SF, Elizabeth AM, Raphael B, Samuel Y, Barry HR, Nicole SB, Stephanie B, Marcel T, Stephen KJ, Viive MH, Brian SH. Biodistribution and Clearance of Stable Superparamagnetic Maghemite Iron Oxide Nanoparticles in Mice Following Intraperitoneal Administration. International Journal of Molecular Sciences. 2018; 19(1):1-205.
6. Kisan Z, Jyoti D, Sushil B, Vikas M, Guruling S. Superparamagnetic Manganese Ferrite Nanoparticles: Synthesis and Magnetic Properties, Journal of Nanoscience and Nanoengineering. 2015; 1(3):178-82.
7. Singh M, Sud SP. Controlling the properties of magnesium-manganese ferrites. Materials Science and Engineering: B. 2001; 83(1-3):180-4. Crossref.
8. Lakshman A, Rao KH, Mendiratta RG. Magnetic properties of In and Cr substituted Mg-Mn ferrites. Journal of Magnetism and Magnetic Materials. 2002; 250:92-7. Crossref.
9. Ahmed MA, El-Khawas EH, Radwan FA. Dependence of dielectric behaviour of Mn-Zn ferrite on sintering temperature. Journal of Materials Science. 2001; 36(20):5031-5. Crossref.
10. Shanmugavela T, Gokul Rajb S, Ramesh Kumarc G, Rajarajana G. Synthesis and Structural Analysis of Nanocrystalline MnFe2O4. Physics Procedia. 2014; 54:159-63 Crossref.
11. Scholten GKD, Usadel KD, Nowak U. Coercivity and exchange bias of ferromagnetic/antiferromagnetic multilayers. Physical Review B. 2004; 71(6-1):064413
12. Gnanaprakash G, Philip J, Raj B. Effect of divalent metal hydroxide solubility product on the size of ferrite nanoparticles. Materials Letters. 2007; 61(23-24):4545-8. Crossref.
13. Jana D, Radim H, Vojtech A, Rene K, Oldrich S, Jaromir H. Preparation and Properties of Various Magnetic Nanoparticles. Sensors. 2009; 9(4):2352-62. Crossref. PMid:22574017 PMCid:PMC3348843.
14. Ananthapadmanabha GS, Vikrant VD. Thermal Properties of Acrylonitrile Butadiene Styrene Composites. Indian Journal of Advances in Chemical Science S1. 2016; p. 279-82.
15. Udayakumar S, Renuka V, Kavitha K. Structural, optical and thermal studies of cobalt doped hexagonal ZnO by simple chemical precipitation method. Journal of Chemical and Pharmaceutical. 2012; 4(2):1271-80.
16. El Sherif M, Terra FS & Khodier SA. Optical characteristics of thin ZnSe films of different thicknesses. Journal of Materials Science: Materials in Electronics. 1996; 7(6): 391-5. Crossref.
17. Nada J, Sapra S, Sarma DD. Size-Selected Zinc Sulfide Nanocrystallites: Synthesis, Structure, and Optical Studies. Chemistry of Materials. 2000; 12(4):1018-24. Crossref.
18. Miguel AP, David J, Samuel S-C, Francisco P. Study of the thermal properties of Acrylonitrile Butadiene Styrene-high impact Polystyrene blends with Styrene Ethylene Butylene Styrene. Annals of the Oradea University. Fascicle of Management and Technological Engineering. 2013; 1: 273-6.
19. Suzuki M, Wilkie CA. The thermal degradation of acrylonitrile butadiene-styrene terpolymer as studied by TGA/FTIR. Polymer Degradation and Stability. 1995; 47(2):217-21. Crossref. Crossref.
20. Han DH, Wang JP, Luo HL. Crystallite size effect on saturation magnetization of fine ferrimagnetic particles. Journal of Magnetism and Magnetic Materials. 1994; 136(1-2): 176-82. Crossref.
21. Eivari HA, Rahdar A, Arabi H. Preparation of superparamagnetic iron oxide nanoparticles and investigation their magnetic properties, International Journal of Science and Engineering Investigations. 2012; 1(3):10312-13.
22. Liu C, Rondinone AJ, Zhang ZJ. Synthesis of magnetic spinel ferrite CoFe2O4 nanoparticles from ferric salt and characterization of the size-dependent superparamagnetic properties. Pure and Applied Chemistry. 2000; 72(1-2):37-45. Crossref.
23. Yu S, Chow GM. Carboxyl group (–CO2H) functionalized ferrimagnetic iron oxide nanoparticles for potential bio-applications. Journal of Materials Chemistry. 2004; 14(18):2781-876. Crossref.
24. Gholamreza N, Davood G. Thermal, Magnetic, and Optical Characteristics of ABS-Fe2O3 Nanocomposites. Journal of Applied Polymer Science. 2012; 125(4):3268-74. Crossref.

25. Theivasanthi T, Alagar M. Innovation of Superparamagnetism in Lead Nanoparticles. Physics and Technical Sciences. 2013; 1(3):39-45. Crossref.
26. Shuo Gu, Weidong He, Ming Z, Taisen Z, Yi Jin, Hatem E, Yiwu M, James HD, Michael JW, Edward DT, Lawrence HB. Physical Justification for Negative Remanent Magnetization in Homogeneous Nanoparticles. Scientific Reports. 2014; 4:6267. Crossref. PMid:25183061 PMCid:PMC4152749.
27. Yan X, Xu Y. Negative remanence in magnetic nanostructures. Journal of Applied Physics.1996; 79:6013. Crossref.
28. Aparna R, De Toro JA, Amaral VS, Muniz PJM, Riveiro JM, Ferreira JMF. Exchange bias beyond the superparamagnetic blocking temperature of the antiferromagnet in a Ni-NiO nanoparticulate system. Journal of Applied Physics. 2014; 115:073904. Crossref.